J. Fluid Mech. (2019), *vol.* 871, R3, doi:10.1017/jfm.2019.396

JFM RAPIDS
journals.cambridge.org/rapids

A note on the aerodynamic splashing of droplets

José Manuel Gordillo[1,†] **and Guillaume Riboux**[1]

[1]Área de Mecánica de Fluidos, Departamento de Ingeniería Aeroespacial y Mecánica de Fluidos, Universidad de Sevilla, Avenida de los Descubrimientos s/n 41092, Sevilla, Spain

(Received 21 March 2019; revised 25 April 2019; accepted 5 May 2019;
first published online 24 May 2019)

When a drop of a low-viscosity liquid of radius R impacts against an inclined smooth solid substrate at a velocity V, a liquid sheet of thickness $H_t \ll R$ is expelled at a velocity $V_t \gg V$. If the impact velocity is such that $V > V^*$, with V^* the critical velocity for splashing, the edge of the expanding liquid sheet lifts off from the wall as a consequence of the gas lubrication force at the wedge region created between the advancing liquid front and the substrate. Here we show that the magnitude of the gas lubrication force is limited by the values of the slip length ℓ_μ at the gas–liquid interface and of the slip length $\ell_g \propto \lambda$ at the solid, with λ the mean free path of gas molecules. We demonstrate that the splashing regime changes depending on the value of the ratio ℓ_μ/ℓ_g – a fact explaining the spreading–splashing–spreading–splashing transition for a fixed (low) value of the gas pressure as the drop impact velocity increases (Xu *et al.*, *Phys. Rev. Lett.*, vol. 94, 2005, 184505; Hao *et al.*, *Phys. Rev. Lett.*, vol. 122, 2019, 054501). We also provide an expression for V^* as a function of the inclination angle of the substrate, the drop radius R, the material properties of the liquid and the gas, and the mean free path λ, in very good agreement with experiments.

Key words: aerosols/atomization, breakup/coalescence

1. Introduction

The prediction of the conditions for which a drop impacting a dry solid spreads or breaks into tiny pieces has recently aroused great interest in the fluid mechanics community for its relevance in not only a number of technological applications, such as coating, cleaning or cooling (Mundo, Sommerfeld & Tropea 1995; Staat *et al.* 2015; Visser *et al.* 2015; Josserand & Thoroddsen 2016), but also in natural processes, such as the propagation of contaminants (Lejeune, Gilet & Bourouiba 2018). The present contribution is aimed at improving our understanding of the

† Email address for correspondence: jgordill@us.es

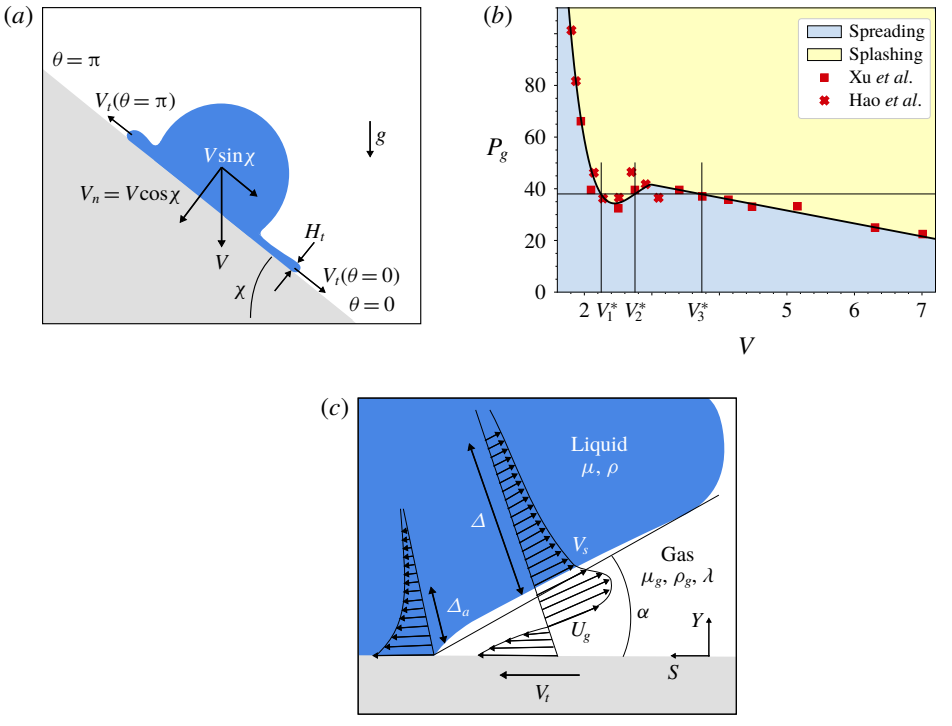

FIGURE 1. (*a*) Sketch showing a drop falling at a velocity V onto a substrate inclined at an angle χ with respect to the horizontal direction and some of the different variables used in the analysis, with θ indicating the angular position on the impact plane. (*b*) Experimental evidence taken from Xu, Zhang & Nagel (2005) and Hao *et al.* (2019) for $\chi = 0$ revealing that, for low values of the atmospheric pressure, with P_g fixed to $P_g = 38$ kPa and increasing values of V, there exists a transition from spreading to splashing for $V = V_1^*$, from splashing to spreading for $V = V_2^*$, and from spreading to splashing for $V = V_3^*$, with $V_1^* < V_2^* < V_3^*$. Experiments corresponding to ethanol droplets in air. (*c*) Sketch of the flow at the edge of the liquid sheet and at the lubrication gas layer in a frame of reference moving at V_t; here, U_g indicates the gas velocity field and V_s is the liquid velocity at the gas–liquid interface. Δ is the width of the viscous boundary layer induced by gas shear stresses and $\Delta_a = R\,\delta \propto R(Re^{-1/2}\,t_e)$ is the thickness of the liquid boundary layer developing at the wall. The material properties of the two fluids involved are also indicated in this figure.

conditions under which a drop falling onto an inclined solid substrate splashes or not; thus, the present situation differs from the similar case in which the drop falls on a pool or thin liquid film (Josserand & Zaleski 2003; Cimpeanu & Moore 2018).

The problem at hand can be stated as follows: a drop of radius R, falling at a velocity V onto an inclined substrate forming an angle χ with respect to the horizontal (see figure 1*a*), will break into smaller parts, rapidly ejected radially outwards, for impact velocities above the critical velocity for splashing, V^*. Our purpose here will be to determine V^* as a function of the drop radius R, the inclination angle χ, the material properties of the liquid, namely, the liquid density, viscosity and interfacial tension coefficient, ρ, μ and σ, respectively, the gas density ρ_g, the gas viscosity μ_g, the mean free path of gas molecules λ, the gas temperature T_g and the gas pressure, P_g. Indeed, in a seminal study, Xu *et al.* (2005) reported that drop splashing could

be inhibited for sufficiently low values of the atmospheric pressure; these results being recently extended to the case of inclined substrates by Hao *et al.* (2019), who also showed that their experimental results could be rationalized on the basis of the value of the velocity V_t at which the lamella is ejected, with V_t calculated using the theoretical results in Riboux & Gordillo (2014) (see figure 1*a*). Moreover, Xu *et al.* (2005), Stevens (2014) and Hao *et al.* (2019) also reported that the threshold velocity for splashing possesses a non-monotonic behaviour for low values of P_g: indeed, for a fixed value of P_g, which must be within a range of values that depends on the material properties of the liquid and the gas, the impacting drop experiences a transition from spreading to splashing for $V \geqslant V_1^*$ but, counterintuitively, splashing is suppressed for values of $V > V_2^*$, with $V_2^* > V_1^*$. Even more surprising is the fact that there exists a further transition from spreading to splashing for $V > V_3^*$ with $V_3^* > V_2^*$ (see figure 1*b*).

This quite unexpected behaviour of droplet splashing at low gas pressures will be explained here by making use of the theory in Riboux & Gordillo (2014) and Riboux & Gordillo (2017), which has been proven to provide good quantitative agreement with experimental measurements (Palacios *et al.* 2013; Staat *et al.* 2015; Hao & Green 2017; de Goede *et al.* 2018; Hao *et al.* 2019). In addition, the remarkable experimental findings in Hao *et al.* (2019) will be expressed here as a function of the drop radius, the inclination angle of the substrate, the material properties of the liquid and the gas, and the values of the gas pressure and gas temperature.

2. Theoretical approach and comparison with experiments

The conditions under which a drop impacting an inclined substrate splashes or not will be expressed as a function of the following dimensionless parameters:

$$Oh = \frac{\mu}{\sqrt{\rho R \sigma}}, \quad Re = \frac{V_n R}{\nu}, \quad We = (Re\, Oh)^2, \quad We_\lambda = We\frac{\lambda}{R}, \tag{2.1a–d}$$

with the normal impact velocity (see figure 1*a*) and the mean free path of gas molecules given by

$$V_n = V\cos\chi \quad \text{and} \quad \lambda = \frac{k_B T_g}{\sqrt{2}\pi d^2 P_g}, \tag{2.2a,b}$$

and where $\nu = \mu/\rho$ denotes the kinematic viscosity of the liquid. In (2.2) k_B denotes the Boltzmann constant, d is the effective diameter of gas molecules, and P_g and T_g indicate the gas pressure and temperature, respectively. Dimensionless variables, which will be written in lower-case letters to differentiate them from their dimensional counterparts – in capitals – are constructed using R, V_n, R/V_n and ρV_n^2 as the characteristic values of length, velocity, time and pressure. Notice that all results will be deduced in a frame of reference moving at the tangential speed of the drop $V\sin\chi$ since, with this choice, an observer would see the drop approximate the wall perpendicularly and with a velocity $V_n = V\cos\chi$. The origin of times, $t = 0$, is set at the instant the drop first touches the substrate and gravitational effects are neglected since the Froude number based on the normal velocity satisfies the condition $V_n^2/(gR) \gg 1$.

In the moving frame of reference, the results in Riboux & Gordillo (2014) and Riboux & Gordillo (2017) are directly applicable and, hence, since $Re^{1/6}Oh^{2/3} < 0.25$ for the case of low-viscosity liquids and millimetric droplets of interest here, a thin

liquid film of dimensionless thickness h_t is not ejected exactly at $t = 0$, but at the instant

$$t_e = 1.05\, We^{-2/3}. \tag{2.3}$$

Moreover, in the moving frame of reference, the initial velocity of the advancing liquid film predicted in Riboux & Gordillo (2014) and Riboux & Gordillo (2017) is given by

$$V_t = V \cos\chi\, v_a \quad \text{with } v_a = \sqrt{3}/2 t_e^{-1/2} \propto We^{1/3} \tag{2.4}$$

and, in the limit $Re \to \infty$, potential flow theory (Scolan & Korobkin 2003; Riboux & Gordillo 2014) predicts that, initially, the thickness of the lamella is given by

$$H_a = R h_a \quad \text{with } h_a = 2t_e^{3/2}/(\sqrt{3}\pi) \propto We^{-1}, \tag{2.5}$$

where use of (2.3) has been made. However, the initial thickness of the ejected sheet is larger than h_a in (2.5) (that is, $h_t > h_a$), because a boundary layer develops upstream of the location where the ejected liquid sheet meets the drop. This boundary layer grows along a characteristic length $h_a \propto t_e^{3/2}$ (see (2.5)) and, since the liquid velocity in the moving frame of reference is, in this region, $v_a \propto t_e^{-1/2}$ (see (2.4)), the thickness of the boundary layer growing at the wall is given by (see figure 1*c*) (Riboux & Gordillo 2015)

$$\Delta_a \propto \sqrt{\nu R/V_n (h_a/v_a)} \propto R\, Re^{-1/2} (h_a/v_a)^{1/2} \propto R\, Re^{-1/2} t_e. \tag{2.6}$$

Hence, mass conservation yields (Riboux & Gordillo 2017)

$$h_t = h_a + \Delta_a/(2R) \propto t_e^{3/2}(1 + K_a/\sqrt{Re\, t_e}) \propto We^{-1}(1 + K_a We^{1/12}\, Oh^{1/2}), \tag{2.7}$$

with $Re = We^{1/2} Oh^{-1}$, $K_a \sim O(1)$ a proportionality constant and where use of (2.3) has been made.

In Riboux & Gordillo (2014) and Riboux & Gordillo (2017) it was also shown that, once the liquid sheet is expelled, its edge experiences a vertical lift force per unit length $F_L \sim \mu_g V_t$ caused by the gas lubrication layer located beneath the liquid rim, which induces a vertical velocity to the front of the expanding liquid sheet

$$V_v \propto \sqrt{F_L/(\rho H_t)} \tag{2.8}$$

in a characteristic time given by

$$T_c \sim \left[\frac{\rho H_t^3}{F_L}\right]^{1/2} \sim \left[\frac{\rho H_t^3}{\mu_g V_t}\right]^{1/2}. \tag{2.9}$$

The vertical velocity imparted to the edge of the expanding sheet could make the lamella take off from the substrate if this velocity is larger than the radial growth of the rim caused by capillary retraction, whose characteristic velocity is given by $\propto\sqrt{\sigma/(\rho H_t)}$; hence, the critical velocity for splashing can be determined from the condition

$$\sqrt{\frac{F_L}{2\sigma}} = \beta, \tag{2.10}$$

with β a constant. In Riboux & Gordillo (2014) and Riboux & Gordillo (2017), the lift force F_L was expressed as the addition of the lubrication force exerted by the gas flow in the wedge region formed by the advancing liquid sheet and the

substrate, $K_l\mu_g V_t$, with V_t the relative velocity between the gas and the liquid, plus the aerodynamic force $K_u\rho_g V_t^2 H_t$, with $K_u = 0.3$ a constant. As was already noticed in Riboux & Gordillo (2014), the relative importance of the aerodynamic lift is always small compared with the lubrication force. In this regard, in our attempt to reproduce the experimental results by Hao *et al.* (2019), we realized (see the supplementary material available at https://doi.org/10.1017/jfm.2019.396 for details) that we overestimated the value of the constant K_u, which we set in this contribution to zero – a fact yielding that the splash criterion in Riboux & Gordillo (2014) and Riboux & Gordillo (2017) can be simplified to

$$\frac{K_l\mu_g V_t}{\sigma} = K \quad \text{with } K = 2\beta^2 - 0.3\rho_g V_t^2 H_t/\sigma \simeq 0.034, \tag{2.11}$$

where we have taken into account that $\beta = 0.14$ and also that, for the experiments reported in Riboux & Gordillo (2014), $0.3\rho_g V_t^2 H_t/\sigma \simeq 0.005$.

Now, we extend our previous results, summarized in the equations above, to the case of inclined substrates and take into account that the relative velocity between the edge of the advancing liquid sheet and the gas is, in dimensionless terms, $v_t = v_a + \tan\chi\cos\theta$, with v_a given in (2.4) (see figure 1*a*, where θ is defined). Making use of the definitions of the different dimensionless variables in (2.1) and of (2.3)–(2.7), the splash criterion (2.11) can be written as

$$K_l\left(\frac{\mu_g}{\mu}\right) Oh\, We^{5/6}[1 + 2(t_e^{1/2}/\sqrt{3})\tan\chi\cos\theta] = K \simeq 0.034. \tag{2.12}$$

The expression for the coefficient K_l in (2.11) results from the integration of the lubrication pressure in the wedge formed between the substrate and the advancing liquid front that propagates at a velocity V_t with respect to the solid wall (see figure 1*c*). The lubrication equations are solved subject to the following boundary conditions in the moving frame of reference:

$$Y = 0: \quad U_g = V_t + \ell_g\frac{\partial U_g}{\partial Y}, \quad Y = H(S): \quad U_g = -\ell_\mu\frac{\partial U_g}{\partial Y}, \tag{2.13a,b}$$

with U_g the gas velocity, and ℓ_g and ℓ_μ representing the slip lengths at the boundaries of the wedge. While ℓ_g is the slip length associated with the Knudsen layer at $Y = 0$ (the so-called Maxwell slip) and, hence, $\ell_g = \lambda$, the slip at $Y = H$ has two different sources: namely, the effect of the Knudsen layer at the gas–liquid interface (Sprittles 2015) plus the velocity induced in the liquid by the gas shear at the interface; therefore, $\ell_\mu = \ell_g + \ell'_\mu$, with ℓ'_μ to be determined in what follows using the balance of shear stresses. The criterion for droplet splashing in (2.12) depends on the gas lubrication force on the advancing liquid wedge, and this force depends crucially on the slip lengths ℓ_g and ℓ_μ in (2.13): indeed, if $\ell_g = \ell_\mu = 0$, the resulting lubrication force would diverge logarithmically up to infinity (Snoeijer & Andreotti 2013).

The solution of the lubrication equations subject to the boundary conditions (2.13) yields the following expression for K_l (see Riboux & Gordillo (2014), Riboux & Gordillo (2017) for details):

$$K_l \approx -(6/\tan^2\alpha)aC_2[\ln(1+a) + \ln a^{-1}] - (6/\tan^2\alpha)bC_3[\ln(1+b) + \ln b^{-1}]. \tag{2.14}$$

In Riboux & Gordillo (2014) and Riboux & Gordillo (2017) we used our experimental results on the splashing of droplets impacting partially wetting substrates, finding that $\alpha \simeq 60°$, $6/\tan^2\alpha \approx 2$. In (2.14), the coefficients a and b are defined as

$$\left.\begin{aligned} a &= 2(\bar{\ell}_g + \bar{\ell}_\mu) + 2\sqrt{(\bar{\ell}_g - \bar{\ell}_\mu)^2 + \bar{\ell}_g\bar{\ell}_\mu} \\ b &= 2(\bar{\ell}_g + \bar{\ell}_\mu) - 2\sqrt{(\bar{\ell}_g - \bar{\ell}_\mu)^2 + \bar{\ell}_g\bar{\ell}_\mu}, \end{aligned}\right\} \tag{2.15}$$

with

$$\left.\begin{aligned} C_1 = \frac{2\bar{\ell}_\mu}{ab}, \quad C_2 = \frac{1 - C_1 b}{b - a}, \quad C_3 = -(C_1 + C_2) \\ \bar{\ell}_g = \lambda/H_t \quad \bar{\ell}_\mu = \bar{\ell}_g + \bar{\ell}'_\mu = \lambda/H_t + \ell'_\mu/H_t. \end{aligned}\right\} \tag{2.16}$$

In (2.16),

$$\bar{\ell}_g \propto \frac{\lambda}{H_t} \propto \left[\frac{\lambda}{R}\right] We(1 + K_a\, We^{1/12}\, Oh^{1/2})^{-1} = We_\lambda(1 + K_a\, We^{1/12}\, Oh^{1/2})^{-1}, \tag{2.17}$$

with h_t and We_λ defined in (2.7) and (2.1), respectively, and $\ell_\mu = \ell_g + \ell'_\mu$, with ℓ'_μ deduced making use of the continuity of shear stresses at the gas–liquid interface: namely,

$$\mu\frac{V_s}{\Delta} \sim \mu_g\frac{\partial U_g}{\partial Y} \implies V_s \sim \left[\Delta\frac{\mu_g}{\mu}\right]\frac{\partial U_g}{\partial Y} = \ell'_\mu\frac{\partial U_g}{\partial Y} \quad \text{with } \ell'_\mu = \Delta\frac{\mu_g}{\mu}. \tag{2.18}$$

In (2.18), Δ denotes the thickness of the boundary layer induced by the gas shear stresses acting on the edge of the ejected liquid sheet, and V_s and U_g indicate, respectively, the velocity at the gas–liquid interface and the gas velocity in the wedge region (see figure 1*c*). At this point, notice that, in Riboux & Gordillo (2014) and Riboux & Gordillo (2017) the slip length at $Y = H$ was approximated as $\ell_\mu = H_t\mu_g/\mu$, which contrasts with $\ell_\mu = \ell_g + \Delta\mu_g/\mu$ used here. Indeed, in our previous contributions we did not take into account the effect of the Knudsen layer at the gas–liquid interface (Sprittles 2015) and also assumed that the momentum diffused so efficiently that the boundary layer thickness coincided with that of the liquid wedge (that is, $\Delta = H_t$).

The boundary layer thickness can be expressed as $\Delta \propto \sqrt{\nu T_c}$, with T_c given in (2.9),

$$\Delta \propto \sqrt{\nu T_c} \propto \sqrt{\nu\left[\frac{\rho H_t^3}{\mu_g V_t}\right]^{1/2}} \propto H_t\left[\frac{\mu}{\mu_g}\right]^{1/4} Re^{-1/4}t_e^{-1/4} \approx H_t\left[\frac{\mu}{\mu_g}\right]^{1/4} Oh^{1/4}, \tag{2.19}$$

where we have made use of the fact that $Re = \sqrt{We}/Oh$ and also of (2.3). Consequently, making use of the definition of ℓ'_μ in (2.18) and of the definitions of $\bar{\ell}_\mu$ and $\bar{\ell}_g$ in (2.16),

$$\bar{\ell}_\mu = \frac{\ell_g}{H_t} + \frac{\ell'_\mu}{H_t} = \bar{\ell}_g + \left[\frac{\mu}{\mu_g}\right]^{-3/4} Oh^{1/4}, \quad \bar{\ell}_g \propto We_\lambda(1 + K_a\, We^{1/12}\, Oh^{1/2})^{-1}. \tag{2.20a,b}$$

In the limit $\bar{\ell}_g/\bar{\ell}_\mu \ll 1 \equiv We_\lambda \ll [\mu_g/\mu]^{3/4}Oh^{1/4}$, with We_λ defined in (2.1), the approximate values of the constants in (2.15) are $a \simeq 4\bar{\ell}_\mu$, $b \simeq 3\bar{\ell}_g$ and hence, since

$-aC_2 = -bC_3 = 1/2$ (see (2.16)), the expression for K_l in (2.14) can be simplified to

$$K_l \simeq \ln[A(\bar{\ell}_\mu \bar{\ell}_g)^{-1}] = \ln\left[A\left(\frac{\mu}{\mu_g}\right)^{3/4} Oh^{-1/4}\, We_\lambda^{-1}\right], \tag{2.21}$$

where we have made use of (2.20), we have assumed that $6/\tan^2\alpha = 2$, A is a fitting constant, and where the term proportional to K_a in (2.20) has been neglected in this case because $Oh \ll 1$.

However, when $\bar{\ell}_g \gtrsim \bar{\ell}'_\mu \equiv We_\lambda \gtrsim [\mu_g/\mu]^{3/4} Oh^{1/4}$, $a \simeq 6\bar{\ell}_g$, $b \simeq 2\bar{\ell}_g$, $-aC_2 \simeq 1$ and $-bC_3 \simeq 0$ (see (2.15)–(2.16)) then equation (2.14) simplifies in this limit to

$$\begin{aligned} K_l &\simeq 2[\ln(1+6\bar{\ell}_g) + \ln(6\bar{\ell}_g)^{-1}] \simeq 2\left[\ln\left(\frac{H_t}{C\lambda}\right) + \ln\left(1+\frac{C\lambda}{H_t}\right)\right] \\ &\simeq 2\left[\ln\left(\frac{1+K_a\, We^{1/12}\, Oh^{1/2}}{C\, We_\lambda}\right) + \ln\left(1+C\, We_\lambda\right)\right], \end{aligned} \tag{2.22}$$

with C a fitting constant and $6/\tan^2\alpha = 2$.

To check the validity of our description, we compare the splash threshold velocities calculated using (2.12) with the experimental values given in Xu *et al.* (2005), Palacios *et al.* (2013), Riboux & Gordillo (2014), Stevens (2014), de Goede *et al.* (2018) and Hao *et al.* (2019). For that purpose, we calculate K_l using either (2.21) if $We_\lambda < 3[\mu_g/\mu]^{3/4} Oh^{1/4}$ or (2.22) if $We_\lambda > 3[\mu_g/\mu]^{3/4} Oh^{1/4}$. At normal atmospheric conditions, ℓ_g is rather smaller than ℓ'_μ and, hence, K_l is calculated using (2.21). Figure 2(*a*) shows that the agreement between experiments and predictions is excellent for the vast majority of fluids investigated: including ethanol, water–ethanol mixtures, water–glycerol mixtures and pure water (see table 1). There are cases, however, in which the agreement between theory and experiments is not so good – and even poor. Indeed, the open symbols in figure 2(*a*), which represent the splashing velocity of water droplets impacting superhydrophobic substrates, notably deviate from the values of V^* predicted using (2.12). The reason for this discrepancy relies on the fact that, for this type of substrate, the edge of the expanding liquid rim is never in contact with the solid and the equation describing the splash transition notably differs from (2.12), as is explained in Quintero, Riboux & Gordillo (2019), where an excellent agreement between the predicted and measured values of V^* is reported.

This example clearly shows that splashing is influenced by the wetting properties of the solids used; this fact being further confirmed by the experimental results in de Goede *et al.* (2018), who found, for the case of partially wetting substrates, that the splash threshold velocity increases slightly for decreasing values of the static contact angle (see figures 2*a*,*b*). This trend is also observed in the experimental points corresponding to methanol and acetone – liquids with very small values of the viscosity and for which the static contact angle is close to zero (see the lighter symbols in figure 2*a*). All the experimental evidence indicates that the wedge angle α is influenced by the wetting properties of the substrate: indeed, it is shown in figure 2(*b*) and is further checked in the supplementary material that the predicted values of V^* would perfectly reproduce the experimental ones if α was allowed to vary within the range of values $60° \pm 3.6°$ (i.e. within a 6 % of variation around 60°). In figure 2(*b*), notice that the larger values of α correspond to the smaller values of the static contact angle and to the smaller values of the liquid viscosity. Thus, the dependence of α on the wetting properties of the solid and the material properties

Ref.	Symbol	ρ (kg m^{-3})	σ (mN m^{-1})	μ (cP)	V^* (m s^{-1})	Re (–)	$Oh \times 10^{-3}$ (–)	Type
(*a*) [1]	●	789	24.0	0.3	3.12	7677	2.4	Glass
(*b*) [1]	●	1000	70.0	1.00	3.68	7211	2.7	Glass
[1]	◆	1000	70.0	1.00	3.70	6421	2.9	Glass
[1]	▶	1000	70.0	1.00	3.98	6491	3.0	Glass
[1]	●	1000	70.0	1.00	4.13	5971	3.1	Glass
(*c*) [1]	★	791	23.0	0.54	2.20	4924	3.2	Glass
[1]	★	791	23.0	0.54	2.74	4237	3.9	Glass
(*d*) [1]	■	789	22.6	1.0	1.77	2130	6.1	Glass
[1]	■	789	22.6	1.0	2.19	1834	7.3	Glass
(*e*) [1]	◀	854	17.2	1.3	1.56	1400	9.1	Glass
[1]	◀	854	17.2	1.3	1.71	988	11.4	Glass
(*f*) [1]	▼	875	17.8	1.7	1.55	1062	12.0	Glass
[1]	▼	875	17.8	1.7	1.81	830	14.7	Glass
[2]	●	989	56.4	1.23	3.83	3394	5.0	Parafilm
[2]	◀	982	48.1	1.50	3.54	2548	6.6	Parafilm
[2]	■	975	42.7	1.82	2.79	1492	8.9	Parafilm
[2]	◆	969	38.0	2.14	2.87	1233	11.5	Parafilm
[2]	▶	935	30.2	2.85	2.50	738	17.9	Parafilm
[2]	★	891	26.2	2.55	2.48	694	18.6	Parafilm
[2]	▲	843	23.8	1.88	2.34	840	14.8	Parafilm
[2]	▼	789	21.8	1.20	2.26	1186	10.2	Parafilm
[2]	●	989	56.4	1.23	4.68	4146	5.0	Glass
[2]	◀	982	48.1	1.50	3.81	2740	6.6	Glass
[2]	■	975	42.7	1.82	3.22	1724	8.9	Glass
[2]	◆	969	38.0	2.14	2.93	1259	11.5	Glass
[2]	▶	935	30.2	2.85	2.50	739	17.9	Glass
[2]	★	891	26.2	2.55	2.50	700	18.6	Glass
[2]	▲	843	23.8	1.88	2.38	855	14.8	Glass
[2]	▼	789	21.8	1.20	2.28	1198	10.2	Glass
[2]	●	989	56.4	1.23	4.08	3615	5.0	Steel
[2]	◀	982	48.1	1.50	3.98	2868	6.6	Steel
[2]	■	975	42.7	1.82	3.15	1689	8.9	Steel
[2]	◆	969	38.0	2.14	2.90	1246	11.5	Steel
[2]	▶	935	30.2	2.85	2.21	654	17.9	Steel
[2]	★	891	26.2	2.55	2.21	619	18.6	Steel
[2]	▲	843	23.8	1.88	2.18	783	14.8	Steel
[2]	▼	789	21.8	1.20	2.15	1127	10.2	Steel
[3]	●	786	20.5	2.0	1.51	738	14.1	Glass
[3]	◀	805	22.3	1.38	2.32	1045	11.7	Glass
[3]	■	805	22.3	1.38	1.68	1271	9.1	Glass
[3]	◆	1050	60.0	1.78	3.16	3096	5.5	Glass
[3]	▶	792	22.2	0.52	3.27	3893	4.4	Glass
[3]	★	792	22.2	0.52	2.50	4576	3.6	Glass
[3]	▲	1000	70.8	1.00	3.61	6479	2.8	Glass
[4]	✖	791	22.9	1.19	1.77	1356	8.2	Glass
[5]	○	1000	72.0	1.00	1.51	3347	2.5	SHydro
[5]	□	1000	72.0	1.00	1.80	2966	2.9	SHydro
[5]	▷	1000	72.0	1.00	2.21	2507	3.5	SHydro

TABLE 1. Values of the material properties of the liquids, the critical velocities for splashing V^*, the corresponding Reynolds numbers $Re = \rho R V^*/\mu$, the Ohnesorge numbers $Oh = \sqrt{We}/Re = \mu/\sqrt{\rho R \sigma}$ and the type of solid substrate, used to plot figure 2. (*a*) Acetone, (*b*) water, (*c*) methanol, (*d*) ethanol, (*e*) decamethyltetrasiloxane, (*f*) dodecamethylpentasiloxane. The angle formed by the substrate with the horizontal is $\chi = 0$ for [1] Riboux & Gordillo (2014), [2] de Goede *et al.* (2018) and [3] Palacios *et al.* (2013) and $\chi \in [0, \pi]$ for [4] Hao *et al.* (2019). In reference [5] Quintero *et al.* (2019), SHydro means Superhydrophobic.

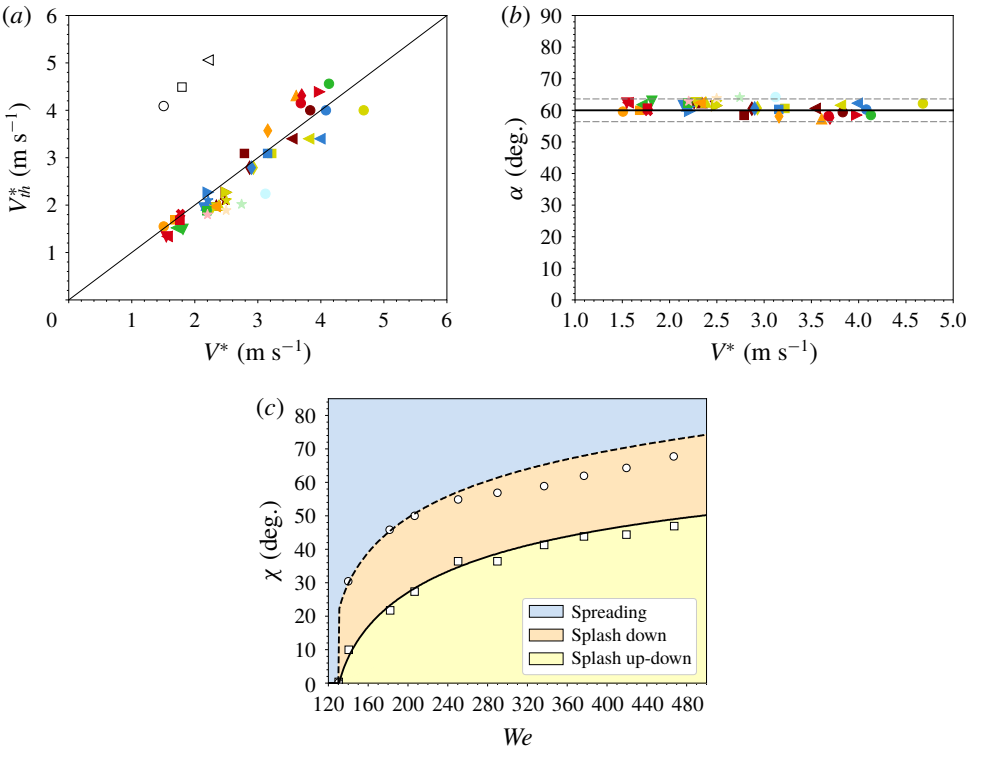

FIGURE 2. (*a*) Comparison between the experimental splash threshold velocities on horizontal substrates at normal atmospheric conditions (see table 1) and the values predicted using (2.12) and (2.21). Open symbols represent the splash threshold velocities on superhydrophobic substrates: the experimental values of V^* corresponding to these cases cannot be predicted by the present theory, but by the one presented in Quintero *et al.* (2019). (*b*) Values of α making the predicted velocity in figure (*a*) coincide with the experimental one (i.e. α is such that $V^*_{th} = V^*$). Observe that, in all cases considered, $\alpha = 60° \pm 3.6°$; namely, the wedge angle varies $\pm 6\,\%$ around 60°. (*c*) Comparison between the experimental splash threshold velocities on inclined substrates measured by Hao *et al.* (2019) at normal atmospheric conditions and the values predicted using (2.12) and (2.21). The symbol (○) and the dashed line represent, respectively, the measured and the calculated velocity for downward splashing ($\theta = 0$), whereas (□) and the continuous line indicate the measured and predicted velocity for upward splashing ($\theta = \pi$) (see figure 1*a*). In (*a–c*), $A = 0.011$, $\alpha = 60°$.

of the liquid is qualitatively similar to that exhibited by the apparent contact angle (Snoeijer & Andreotti 2013). Let us point out that an attempt to link α with the apparent contact angle was already done in Riboux & Gordillo (2014), where the shape of the advancing liquid wedge as well as the value of the critical capillary number were predicted using the theory presented in Marchand *et al.* (2012), which extends the previous theory by Cox (1986). We found, however, that the lubrication approximation predicts that air entrainment is produced for values of the capillary number smaller than those for which the splash transition is experimentally observed. These results led us to conclude in Riboux & Gordillo (2014) that: (i) dewetting is a necessary but not sufficient condition for splashing and also that (ii) the wedge angle

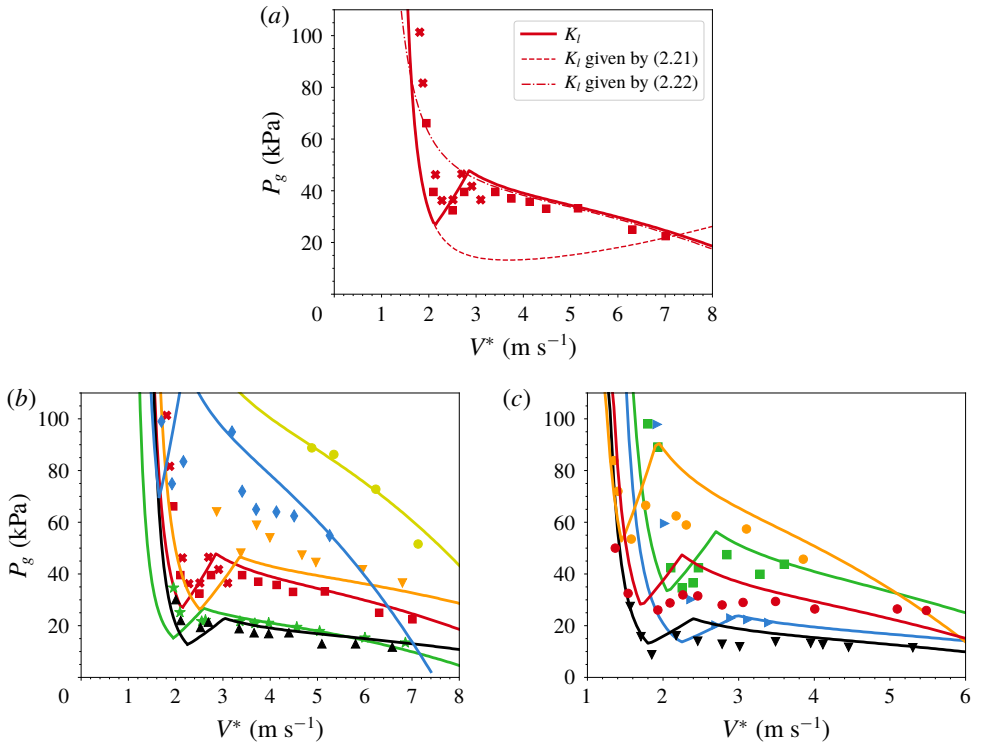

FIGURE 3. (*a*) Comparison between the experimental data in Xu *et al.* (2005) and Hao *et al.* (2019) and the predicted splash threshold velocity using the expressions for K_l given by either (2.21) or by (2.22). (*b*,*c*) Comparison between the experimental splash threshold velocities at reduced atmospheric conditions measured by Xu *et al.* (2005), Stevens (2014) and Hao *et al.* (2019) (see table 2), and the values predicted using (2.12), (2.21) and (2.22). In (*a–c*), $\chi = 0$, $\alpha = 60°$, $A = 0.011$, $C = 19$ and $K_a = 0.7$. The deviations observed between the predicted and experimental values corresponding to orange symbols in panels (*b*) and (*c*) can be attributed to slight variations of the wedge angle α (see the supplementary material for details).

α cannot be calculated using either the lubrication theory in Riboux & Gordillo (2014) or the more recent by Kamal *et al.* (2019). Indeed, the lubrication approximation is not adequate to describe the flow at the wedge because the time scales associated with droplet splashing are so short that viscous effects in the liquid are confined to thin boundary layers (as sketched in figure 1*c*), whereas, in Stokes flow, the momentum diffuses so efficiently across the liquid that boundary layers do not exist. Therefore, new theories retaining inertia and the highly transient nature of splashing or, alternatively, simulations of the type reported in Sprittles (2017) would be needed to predict the value of α as a function of the wetting properties of the solid substrate and the material properties of the two fluids involved.

This said, in spite of its simplicity, our model is in good agreement with the experimental measurements depicted in figure 2(*a*) and nicely reproduces the experimental splash transition on inclined substrates reported by Hao *et al.* (2019) (see figure 2*c*); the good agreement between experiments and predictions is also captured by the modification in Hao *et al.* (2019) of our original analysis in Riboux

Ref.	Fig.	Gas	Symbol	$\lambda_0 \times 10^{-9}$ (m)	$\mu_g \times 10^{-5}$ (Pa s)	ρ_{g0} (kg m^{-3})	ρ (kg m^{-3})	σ (mN m^{-1})	μ (cP)	$Oh \times 10^{-3}$ (–)
[1]	3(*b*)	Helium	●	193	1.98	0.16	789	22.4	1.04	6.0
[1]	3(*a*,*b*)	Air	■	68	1.85	1.18	789	22.4	1.04	6.0
[1]	3(*b*)	Krypton	★	58	2.51	3.42	789	22.4	1.04	6.0
[1]	3(*b*)	SF_6	▲	25	1.53	6.04	789	22.4	1.04	6.0
[1]	3(*b*)	Air	▼	68	1.85	1.18	791	23.5	0.54	3.0
[2]	3(*a*,*b*)	Air	✖	68	1.85	1.18	791	22.9	1.19	8.2
[3]	3(*c*)	Helium	◆	193	1.98	0.16	840	18.7	1.7	10.7
[3]	3(*c*)	Air	●	68	1.85	1.18	1860	16.0	1.8	11.7
[3]	3(*c*)	Air	●	68	1.85	1.18	765	19.7	2.3	14.8
[3]	3(*c*)	Air	■	68	1.85	1.18	755	19.0	1.8	16.8
[3]	3(*c*)	SF_6	▶	25	1.53	6.04	750	18.0	1.1	10.0
[3]	3(*c*)	SF_6	▼	25	1.53	6.04	840	18.7	1.7	10.7

TABLE 2. Physical properties of the different liquids and gases used to plot figure 3. Here, $T_{g0} = 298.15$ K and $P_{g0} = 10^5$ Pa. Therefore, for arbitrary values of the gas temperature T_g and pressure P_g, $\lambda = \lambda_0 (T_g/T_{g0})(P_{g0}/P_g)$. [1] Xu *et al.* (2005), [2] Hao *et al.* (2019) and [3] Stevens (2014).

& Gordillo (2014). In addition, our theory also predicts the spreading–splashing–spreading–splashing transition for reduced atmospheric pressures and increasing impact velocities, first reported by Xu *et al.* (2005) and later confirmed by Stevens (2014) and Hao *et al.* (2019) (see figure 3). Indeed, for the larger values of P_g, the curves in solid lines in figure 3 have been calculated as those in figure 2, using (2.21) with $A = 11 \times 10^{-3}$ but, since the mean free path of gas molecules varies with pressure as $\lambda \propto P_g^{-1}$, the slip length at the solid wall becomes larger than ℓ'_μ for reduced pressures and hence, when $We_\lambda > 3[\mu_g/\mu]^{3/4} Oh^{1/4}$, K_l is calculated using (2.22), with $C = 19.0$ and $K_a = 0.7$. Notice that, under rarefied gas conditions, the effect of the boundary layer thickness, quantified through the term proportional to K_a in (2.22), needs to be retained in the expression of K_l.

The physical interpretation of the results depicted in figure 3, which illustrate the non-monotonicity of the splash threshold velocity at reduced atmospheric pressures, is provided in what follows. First, notice that the vertical lubrication force would diverge logarithmically up to infinity if the slip lengths ℓ_g and ℓ'_μ were equal to zero, but the existence of slip at both the wall and at the gas–liquid interface limits the value of the lubrication force (see (2.14)–(2.15)). The lift force is bounded by the maximum value of either ℓ'_μ or ℓ_g, which are roughly given by (see (2.2) and (2.20))

$$\ell'_\mu \sim H_l (\mu_g/\mu)^{3/4} Oh^{1/4} \sim R\, We^{-1} (\mu_g/\mu)^{3/4} Oh^{1/4} \quad \text{and} \quad \ell_g \propto \lambda \propto \lambda_0 (P_{g0}/P_g). \tag{2.23a,b}$$

For gas pressures P_g of the order of, or slightly below $P_{g0} \simeq 100$ kPa, ℓ_g is $\sim 10^{-7}$ m and, thus, $\ell_g \ll \ell'_\mu$. Hence, for moderate values of P_g, the lubrication force on the wedge is bounded by the slip at the gas–liquid interface associated with the balance of shear stresses. When this happens, the lubrication lift force $K_l \mu_g V_t$ depends on P_g weakly through λ (see (2.21)) – this being the reason for the large slope of the $P_g - V^*$ curve depicted in figure 3(*a*). However, for a fixed value of P_g sensibly smaller than P_{g0}, say $P_g \sim 30$ kPa ($\lambda > \lambda_0$ is fixed) and increasing impact velocities, $\ell_g > \ell'_\mu$ – a fact yielding that the coefficient K_l in the lubrication lift force, $K_l \mu_g V_t$, decreases strongly when the mean free path becomes of the order of the thickness of the lamella;

namely, when the ratio λ/H_t increases and becomes of order unity (see (2.22)–(2.23)). Therefore, for low values of the gas pressure P_g and impact velocities V such that H_t is very small and $\ell_g \sim \ell'_\mu$, the lift force decreases abruptly – a fact explaining the transition from splashing to spreading. However, for even larger impact velocities, the lubrication lift force $K_l \mu_g V_t$ increases with V because K_l decreases with V but only logarithmically – a fact explaining the second transition from spreading to splashing for very large impact velocities.

As a final remark, let us point out that the theoretical approach presented here, obtained by setting the multiplicative constant K_u affecting the aerodynamic lift term $K_u \rho_g V_t^2 H_t$ equal to zero, is a simplification revealing that we overestimated the relative importance of this term in Riboux & Gordillo (2014), where we reported that $K_u = 0.3$. But the approach used here does not mean that, in physical terms, the aerodynamic lift is zero: indeed, Jian *et al.* (2018) confirmed numerically our original result that splashing can be enhanced thanks to the aerodynamic lift. This conclusion is further supported in the supplementary material, where the comparison with the experimental results by Hao *et al.* (2019) reveals that the magnitude of K_u is only 10 % of the value we provided in Riboux & Gordillo (2014) – a fact explaining why the available experiments in the literature can be explained by setting $K_u = 0$.

3. Concluding remarks

Making use of the model developed in Riboux & Gordillo (2014) and Riboux & Gordillo (2017), and thanks to the recent experimental results obtained by Hao *et al.* (2019), here we provide a more accurate expression for the lift force exerted by the gas on the edge of the expanding lamella. We have shown that the expression for the lift force depends crucially on the value of the ratio ℓ'_μ/ℓ_g, with ℓ'_μ the slip length at the gas–liquid interface and ℓ_g the slip length at the solid wall. It is precisely when $\ell'_\mu \sim \ell_g$ that drops falling on a smooth substrate exhibit the spreading–splashing–spreading–splashing transition for a fixed value of the atmospheric pressure and increasing values of the impact velocity already reported by Xu *et al.* (2005), Stevens (2014) and Hao *et al.* (2019).

In addition, we provide an equation expressing the splash threshold velocity V^* as a function of the inclination angle of the substrate, the drop radius R, the material properties of the liquid and the gas, and the mean free path of gas molecules, which is in good quantitative agreement with experiments.

Acknowledgements

This work has been supported by the Spanish MINECO under Project DPI2017–88201–C3–1–R, partly financed through European funds.

Supplementary material

Supplementary material is available at https://doi.org/10.1017/jfm.2019.396.

References

CIMPEANU, R. & MOORE, M. R. 2018 Early-time jet formation in liquid–liquid impact problems: theory and simulations. *J. Fluid Mech.* **856**, 764–796.

COX, R. G. 1986 The dynamics of the spreading of liquids on a solid surface. Part 1. Viscous flow. *J. Fluid Mech.* **168**, 169–194.

DE GOEDE, T. C., LAAN, N., DE BRUIN, K. G. & BONN, D. 2018 Effect of wetting on drop splashing of Newtonian fluids and blood. *Langmuir* **34** (18), 5163–5168.

HAO, J. & GREEN, S. I. 2017 Splash threshold of a droplet impacting a moving substrate. *Phys. Fluids* **29**, 012103.

HAO, J., LU, J., LEE, L., WU, Z., HU, G. & FLORYAN, J. M. 2019 Droplet splashing on an inclined surface. *Phys. Rev. Lett.* **122**, 054501.

JIAN, Z., JOSSERAND, C., POPINET, S., RAY, P. & ZALESKI, S. 2018 Two mechanisms of droplet splashing on a solid substrate. *J. Fluid Mech.* **835**, 1065–1086.

JOSSERAND, C. & THORODDSEN, S. T. 2016 Drop impact on a solid surface. *Annu. Rev. Fluid Mech.* **48**, 365–391.

JOSSERAND, C. & ZALESKI, S. 2003 Droplet splashing on a thin liquid film. *Phys. Fluids* **15**, 1650–1657.

KAMAL, C., SPRITTLES, J. E., SNOEIJER, J. H. & EGGERS, J. 2019 Dynamic drying transition via free-surface cusps. *J. Fluid Mech.* **858**, 760–786.

LEJEUNE, S., GILET, T. & BOUROUIBA, L. 2018 Edge effect: liquid sheet and droplets formed by drop impact close to an edge. *Phys. Rev. Fluids* **3**, 083601.

MARCHAND, A., CHAN, T. S., SNOEIJER, J. H. & ANDREOTTI, B. 2012 Air entrainment by contact lines of a solid plate plunged into a viscous fluid. *Phys. Rev. Lett.* **108**, 204501.

MUNDO, C., SOMMERFELD, M. & TROPEA, C. 1995 Droplet-wall collisions: experimental studies of the deformation and breakup process. *Intl J. Multiphase Flow* **21**, 151–173.

PALACIOS, J., HERNANDEZ, J., GOMEZ, P., ZANZI, C. & LOPEZ, J. 2013 Experimental study of splashing patterns and the splashing/deposition threshold in drop impacts onto dry smooth solid surfaces. *Exp. Therm. Fluid Sci.* **44**, 571–582.

QUINTERO, E. S., RIBOUX, G. & GORDILLO, J. M. 2019 Splashing of droplets impacting superhydrophobic substrates. *J. Fluid Mech.* **870**, 175–188.

RIBOUX, G. & GORDILLO, J. M. 2014 Experiments of drops impacting a smooth solid surface: a model of the critical impact speed for drop splashing. *Phys. Rev. Lett.* **113**, 024507.

RIBOUX, G. & GORDILLO, J. M. 2015 The diameters and velocities of the droplets ejected after splashing. *J. Fluid Mech.* **772**, 630–648.

RIBOUX, G. & GORDILLO, J. M. 2017 Boundary-layer effects in droplet splashing. *Phys. Rev.* E **96**, 013105.

SCOLAN, Y. M. & KOROBKIN, A. A. 2003 Energy distribution from vertical impact of a three-dimensional solid body onto the flat free surface of an ideal fluid. *J. Fluids Struct.* **17**, 275–286.

SNOEIJER, J. H. & ANDREOTTI, B. 2013 Moving contact lines: scales, regimes, and dynamical transitions. *Annu. Rev. Fluid Mech.* **45**, 269–292.

SPRITTLES, J. E. 2015 Air entrainment in dynamic wetting: Knudsen effects and the influence of ambient air pressure. *J. Fluid Mech.* **769**, 444–481.

SPRITTLES, J. E. 2017 Kinetic effects in dynamic wetting. *Phys. Rev. Lett.* **118**, 114502.

STAAT, H. J. J., TRAN, T., GEERDINK, B., RIBOUX, G., SUN, C., GORDILLO, J. M. & LOHSE, D. 2015 Phase diagram for droplet impact on superheated surfaces. *J. Fluid Mech.* **779**, R3.

STEVENS, C. S. 2014 Scaling of the splash threshold for low-viscosity fluids. *Europhys. Lett.* **106**, 24001.

VISSER, C. W., FROMMHOLD, P. H., WILDEMAN, S., METTIN, R., LOHSE, D. & SUN, C. 2015 Dynamics of high-speed micro-drop impact: numerical simulations and experiments at frame-to-frame times below 100 ns. *Soft Matt.* **11**, 1708–1722.

XU, L., ZHANG, W. W. & NAGEL, S. R. 2005 Drop splashing on a dry smooth surface. *Phys. Rev. Lett.* **94**, 184505.